Acta Acustica united with Acustica
Vol. 98 (2012) 600 – 610

DOI 10.3813/AAA.918541

Experimental and Numerical Study of Flow over a Cavity for Reduction of Buffeting Noise

Yiping Wang[1,2,3)], Hsu Chew Lee[1)], Kai Ming Li[1)], Zhengqi Gu[2)], Jun Chen[1)]

[1)] Ray W. Herrick Laboratories, School of Mechanical Engineering, Purdue University, West Lafayette, IN 47907, USA. mmkmli@purdue.edu

[2)] State Key Laboratory of Advanced Design and Manufacturing for Vehicle Body, Hunan University, Changsha, Hunan 410082, China

[3)] School of Automobile Engineering, Wuhan University of Technology, Wuhan, Hubei 430070, China

Summary

Experimental and numerical investigations are conducted to investigate the noise induced by a subsonic flow over a cavity. Particular attention is focused on the problem of low-frequency pressure oscillations inside the cabins of automobiles with open sunroofs. The mechanisms of buffeting noise are examined by considering a model cavity. Extensive experiments are performed to validate the computational scheme developed in the present study. This computational scheme is used for designing generic deflectors for reducing buffeting noise. Experimental and computational results show that the traditional generic deflector is unable to reduce the buffeting noise when the flow velocity is sufficiently high. However, a vented deflector allows the effective control of the buffeting noise at relatively high flow speeds.

PACS no. 43.28.Py, 43.50.Lj, 43.50.Nm

1. Introduction

The aerodynamic noise induced by a flow over a cavity is important for aircraft and automobile design. This unsteady noise triggered by an airfoil slat [1] or the landing gear (e.g., [2]) of a cruising vehicle is a major aeroacoustic source [3]. In the case of land-based vehicles, buffeting noise is produced when air flows over sunroofs at low subsonic speeds [4, 5], side-windows [6], or other body cavities. The wind buffeting noise is an aeroacoustic response of the air bulk trapped in the cavity of external transient airflows [7]. It is characterized by a high noise level with a relatively low frequency, ranging from 10 to 50 Hz. Its magnitude may exceed 130 dB, causing unacceptable discomfort to the driver and the passengers [8]. According to Rockwell and Naudascher [9], this phenomenon is attributable to the resonant oscillation of fluids.

An initial survey on automobiles indicated that the wind noise is consistently one of the top consumer complaints that have a direct impact on the consumers' brand loyalty and vehicle sales [10]. Of all consumers' complaints pertaining to automobile noise, 24% is specifically linked to the sunroof buffeting noise (e.g., [5]) that makes its reduction as one of the top priorities for improving passenger comfort.

With the development of computational fluid dynamics (CFD) techniques and the availability of inexpensive computational resources, the use of numerical simulations for studying wind buffeting noise has become more affordable. Unsteady, incompressible Navier–Stokes (N–S) equations are often adopted to predict the buffeting noise characteristics [11]. However, one cannot successfully predict the high noise levels at specific vehicle speeds and in a specific frequency range because the resonant oscillation of fluids cannot be faithfully simulated without accounting for the compressibility effect of the flow [8]. Further, An *et al.* [12] showed that the sound pressure level was underestimated by more than 10 dB and the buffeting frequency was overestimated when the effect of compressibility was not integrated into the numerical analyses.

Hence, the inclusion of compressibility in the numerical analysis is of vital importance for predicting the buffeting noise. On the other hand, one can possibly adopt compressible N–S equations in the simulation of a flow with a low Mach number. The so-called stiffness problem [13] is known to lead to an inefficient and inaccurate implementation of most conventional CFD schemes. To solve the stiffness problem, Inagaki *et al.* [8] derived a set of basic equations from compressible N–S equations. An assumption of the weak compressibility effect was used for correlating the deviation of pressure from the atmospheric pressure. Their simulation results agreed well with the experimental data.

It is well known that buffeting noise is a complex feedback mechanism involving the amplification and convection of small instabilities by the shear layer. The impingement of these flow instabilities at the downstream corner

Received 8 August 2011,
accepted 29 March 2012.

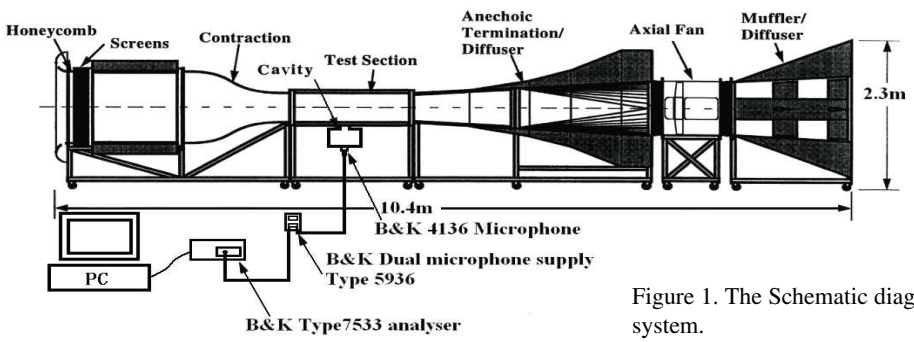

Figure 1. The Schematic diagram of the wind tunnel and test system.

generates acoustic waves. These high-amplitude acoustic waves, in turn, travel upstream and excite further disturbances in the shear layer, leading to a self-sustained oscillation process [9]. It should be pointed out that specific buffeting control methods can work only under certain circumstances. However, many of these proposed methods are not well understood and thus are not effectively utilized [7] to suppress the buffeting noise in a cavity. In this study, an accurate CFD scheme was applied to design an effective deflector for reducing the wind buffeting noise. We wish to explore the method of flow "venting" by introducing a secondary opening in the deflector. Use of the secondary vent may cause unsteady oscillations at other frequencies. However, a more careful design supported by accurate numerical simulations should be sufficient to minimize this potential drawback of introducing the additional opening in the deflector.

The rest of this paper is organized as follows: The experimental setup and the computational scheme are introduced in section 2. In section 3, the validity of the CFD simulations is confirmed by comparing the experimental data with the numerical results for the subsonic flow over a simple cavity. section 4 describes the process of designing a simple deflector and a vented deflector to reduce the wind buffeting noise. Section 5 presents the numerical simulations that are used for examining the mechanism of noise suppression for the simple deflector and the vented deflector. The conclusions and outlook of the research are given in section 6.

2. Experimental and computational models

2.1. Experimental setup

The experimental facility used in the present study is an acoustically treated small-scale blown-down wind tunnel located at Ray W. Herrick Laboratories of Purdue University (see Figure 1). The wind tunnel consisted of an inlet section, a rectangular test section, and a diffuser section. The inlet section consisted of a settling chamber mounted with honeycomb and layered meshes. A parabolic rectangular contraction was connected from the inlet section to the test section where a uniform velocity profile (within 2%) was obtained at the inlet of the test section. The test section was 1,200 mm long, 450 mm high, and 530 mm wide. The sidewalls and ceiling were made of 25-mm-thick Plexiglas to facilitate flow visualization. The floor was made of 15-mm-thick plywood for easy removal that allowed a rapid installation of experimental rigs and flow control devices. The diffuser section was built with an anechoic termination that served to minimize the sound reflected from the outlet of the wind tunnel. The primary diffuser was connected with the outlet of the test section. An extractor fan was housed within the primary diffuser with the allowable axial distance minimized. The primary diffuser section also served as the principal sound absorption region. The secondary diffuser was designed to further slow the air stream as well as to provide acoustic attenuation. The fan was driven directly by a Reliance Electric 14.9-kW AC motor, and a Reliance Electric variable frequency controller was used for precise fan speed control [14]. The maximum flow velocity achieved was 28 m/s (100 km/h) with 1% span-wise uniformity.

A single-wire hot-wire anemometer was used for measuring the root-mean-square fluctuations of the velocity with the mean value ranging between 13 and 40 m/s. Six locations across a cross-sectional plane, which was located 530 mm from the entrance of the test section, were chosen for the measurements. An average of 0.1% of the mean flow velocity in the frequency varying from 1 Hz to 3 kHz was reported [15]. All connections in the test section were sealed with O-rings in grooves to minimize the acoustic leakage.

An open-top rectangular box with a span-wise width of 0.3 m, length of 0.4 m, and depth of 0.29 m was used as the model cavity (see Figure 2). The volume of the rectangular cavity was chosen with a one-fifth scale comparable to the cavity of a typical automobile's cabin. The front part of vehicle was ignored in the experimental study as the main focus was the development of an effective means to reduce wind buffeting noise.

The model cavity was mounted on the plywood floor of the test section. There was a rectangular aperture with a span-wise width of 240 mm and a length of 100 mm along the centerline on the test section's floor. The leading edge of the rectangular aperture was located at 400 mm downstream of the test-section inlet. The cavity center was aligned with the center of the rectangular aperture. This

model is referred to as Model A in the following sections. Figure 2 shows a schematic representation of Model A.

A Brüel and Kjær type 4236 1/4" microphone was flush mounted at the geometric center on the floor of the cavity. It was used for measuring pressure fluctuations at three different mean flow speeds of 15, 20, and 25 m/s. A Brüel and Kjær type 5936 dual microphone supply was used as the power source for the microphone. A Brüel and Kjær type 7533 pulse frequency analyzer, which was controlled by a desktop computer, was used for analyzing and recording acoustic data for subsequent processing.

2.2. Computational schemes

Assuming a weak compressibility effect for a low-speed flow with no heat sources, Ingaki *et al.* [8] showed that a set of non-dimensional equations can be summarized as

$$M^2\left\{\frac{\partial p}{\partial t}+u_j\frac{\partial p}{\partial x_j}\right\}+\frac{\partial u_j}{\partial x_j}=0, \tag{1a}$$

$$\frac{\partial u_i}{\partial t}+\frac{\partial u_j u_i}{\partial x_j}-u_i\frac{\partial u_j}{\partial x_j}= -\frac{\partial p}{\partial x}+\frac{\partial}{\partial x_j}\left\{\frac{1}{\mathrm{Re}}\left(\frac{\partial u_i}{\partial x_j}+\frac{\partial u_j}{\partial x_i}\right)\right\}, \tag{1b}$$

where M is the Mach number, p is the pressure fluctuation, u_j is the flow velocity in the x_j direction, t is the time variable, and Re is the Reynolds number of the flow. Note that the first term on the left side of equation (1a) accounts for the deviation from the divergence-free condition of an incompressible flow. The density, temperature and sound speed of air are taken as constant because a low Mach number flow is considered in the current analyses.

To obtain numerical solutions for equations (1a) and (1b), researchers frequently use a large eddy simulation (LES) approach [16] on the resolved velocity and pressure in favor of p and u_j. These resolved components ($\overline{u}_j$ and $\overline{p}$) are defined as

$$\overline{u}_j(x,t)=\int_D u_j(x-x*,t)\,G_\Delta(x')\,\mathrm{d}x', \tag{2a}$$

and

$$\overline{p}(x,t)=\int_D p(x-x*,t)\,G_\Delta(x')\,\mathrm{d}x', \tag{2b}$$

where G_Δ is the filtering kernel with a characteristic length scale of Δ. Applying the operator G_Δ in equations (1a) and (1b), we obtained a set of filtered equations,

$$M^2\left\{\frac{\partial \overline{p}}{\partial t}+\overline{u}_j\frac{\partial \overline{p}}{\partial x_j}\right\}+\frac{\partial \overline{u}_j}{\partial x_j}=0, \tag{3a}$$

and

$$\frac{\partial \overline{u}_i}{\partial t}+\overline{u}_j\frac{\partial \overline{u}_i}{\partial x_j}= -\frac{\partial \overline{p}}{\partial x_i}+\frac{1}{\mathrm{Re}}\frac{\partial}{\partial x_j}\left(\frac{\partial \overline{u}_i}{\partial x_j}+\frac{\partial \overline{u}_j}{\partial x_i}\right)-\frac{\partial \tau_{ij}}{\partial x_j}, \tag{3b}$$

where τ_{ij} is the subgrid-scale stresses.

In fact, these two equations were essentially the same as the governing equations for the incompressible LES except for the first term on the left side of equation (3a). This term could be represented by a source term added to the incompressible equations instead. The Smagorinsky–Lilly subgrid-scale stress (SGS) model [17] was employed to close equations (3a) and (3b) as

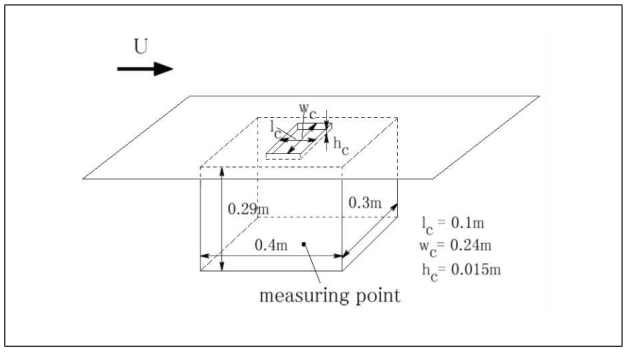

Figure 2. Schematic diagram of the three-dimensional cavity model (Model A).

$$\tau_{ij}-\frac{1}{3}\tau_{kk}\delta_{ij}=-2\mu\overline{S}_{ij}, \tag{4a}$$

where μ_t is the subsgrid scale turbulent viscosity and S_{ij} is the sub-grid scale shear strain tensors. They are given, respectively, by

$$\overline{S}_{ij}=\frac{1}{2}\left(\frac{\partial \overline{u}_i}{\partial x_j}+\frac{\partial \overline{u}_j}{\partial x_i}\right), \tag{4b}$$

and

$$\mu_t=\rho L_s^2\left|\overline{S}\right|, \tag{4c}$$

where L_s is the mixing length for the subgrid scales, and

$$\left|\overline{S}\right|\equiv\sqrt{2\overline{S}_{ij}\overline{S}_{ij}}. \tag{4d}$$

The mixing length L_s was computed using

$$L_s=\min\left(kd, C_sV^{1/3}\right), \tag{4e}$$

where k is the von Karman constant, d is the distance to the closest wall, C_s is the Smagorinsky constant, which is set to 0.1, and V is the volume of the computational cell.

As mentioned before, the weak compressibility effect was accounted for by the additional term in equation (1a). In the present study, a commercially available CFD software package, Fluent, was used. In particular, an incompressible fluid model was used, but the additional term given in equation (1a) was included in the continuity equation as the source term. This could be achieved by a user-defined function (UDF) module in Fluent to predict the fluctuating pressure due to the aeroacoustic noise sources. It should be mentioned that the governing equations solved by Fluent are usually given in the dimensionalized form. However, equations (3a) and (3b) are specified in the non-dimensionalized form. To account for this apparent discrepancy, the density and viscosity of air were set at 1 and 1/Re respectively in running the Fluent CFD program. The

equivalent non-dimensionalized results would then be obtained directly from Fluent's numerical simulations.

An implicit pressure-based finite volume method was used for solving the weakly compressible LES equations on unstructured grids. These unstructured grids around the cavity are shown in Figure 3. Approximately, two million grid points were used in our computations with the minimum and maximum spatial resolutions of 0.01 mm and 20 mm, respectively. The mesh is 'stretched' in direction normal to the wall. The ratio for the number of sampling points in the mutually perpendicular directions to that sampled in the normal direction is 5%.

Specifically, there are twelve nodal points within the viscous sublayer, $y^+ \leq 11.8$, in the normal direction. The first nodal point is chosen at $y^+ = 1.5$. A pressure-implicit algorithm for transient calculations with splitting operators [18] was employed in the numerical solver. This algorithm is based on the conservation form of the momentum equation and the discretized transport equations. The computed field variables were advanced in time with the iterative time-advancement scheme. With this iterative scheme, the splitting error was eliminated because the non-linearity of the individual equations and inter-equation couplings were fully incorporated into the computations. In order to avoid the effect of the numerical diffusion, the convection terms in all transport equations were discretized by using bounded central differencing (BCD) schemes. These schemes served to avoid possible unbounded solutions and non-physical oscillations caused by central-differencing schemes, while preserving the non-dissipative properties. The diffusion terms were central-differenced and always had second-order accuracy. The transient terms were approximated by fully implicit, second-order accurate finite differences. The pressure was interpolated using the pressure staggering option.

The time scale of the smallest resolved eddies in the LES dictates the required size of each time step. Ingaki *et al.* [8] used two different criteria to control for the convergence of the numerical results. The first criterion was based on the smallest size of $10^{-3} l_c$ where l_c is the longitudinal length of the opening. The other criterion employs a step length of $5 \cdot 10^{-4} l_c$. According to their simulations, use of these two criteria led to almost the same numerical results. In light of their numerical results, a step length with the smallest size of a resolved eddy as $10^{-4} l_c$ is chosen in the present study. The non-dimensional time step was, therefore, set as $10^{-3} l_c / U_0$ in the CFD scheme. The computational results showed that the ratio of the turbulent viscosity and the molecular viscosity inside the boundary layer is about 20, and this ratio approaches to zero at the far-field.

Figure 4 shows the computational domain used in the present study. It is worthy of mentioning that the LES predictions are inherently unsteady and dominated by vortical structures. The reflecting boundary conditions, which apply simple extrapolations based on zero or any higher order polynomials along streamlines or grid lines, will lead to unsatisfactory results. The problem of upstream-

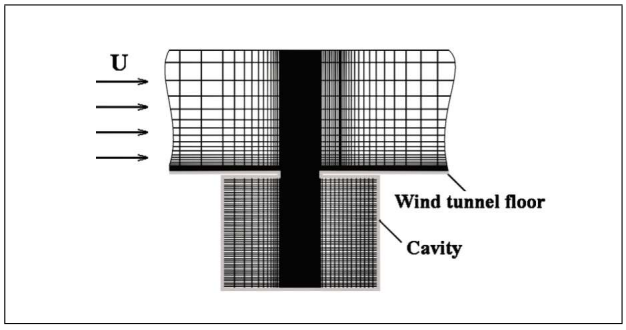

Figure 3. Grids along longitudinal symmetry plane.

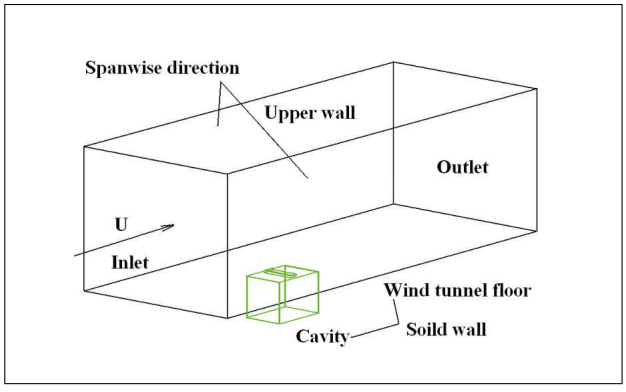

Figure 4. The computational domain of the study.

traveling perturbations triggered by outflow boundary conditions is a topic of continual interest for CFD. Thus, a variety of so-called nonreflecting boundary conditions was used in the current study. Particularly, the convective boundary condition according to Orlanski [19] was used because Breuer [20, 21] showed that this scheme worked extremely well. The other boundary conditions were the continuity of mass at the inlet, no-slip condition, the use of the wall-function method [22] on the floor of the test section, and the use of the slip condition for the ceiling along the spanwise direction.

The wall-function method used an assumed instantaneous velocity profile between the nodes closest to the wall and the wall surface. A popularly used wall function assumed a 1/7th power law outside the viscous sublayer, interfaced with the linear profile in the viscous sublayer (Werner–Wengle wall functions proposed by Werner *et al.* [23]).

$$u^+(y) = \begin{cases} y^+ & \text{if} \quad y^+ < 11.8, \\ 8.3(y^+)^{1/7} & \text{if} \quad y^+ > 11.8. \end{cases} \tag{5}$$

The tangential velocity components could be related to the corresponding wall shear stress by integrating the velocity profile given above over the distance separating the first cell from the wall. Other wall functions, e.g., the logarithmic profile, have been used in other studies, but they will not be considered here.

Table I. Predicted and measured resonant modal frequencies.

Velocity (m/s)	Rossiter (Hz)				Experiment (Hz)				Simulations (Hz)			
	$n = 1$	$n = 2$	$n = 3$	$n = 4$	$n = 1$	$n = 2$	$n = 3$	$n = 4$	$n = 1$	$n = 2$	$n = 3$	$n = 4$
15	61.1	122.2	183.3	244.5	62.3	122.0	185.5	244.3	57.6	114.0	171.3	228.6
20	81.4	162.8	244.2	325.7	83.0	166.5	249.5	333.3	83.6	167.9	250.1	334.6
25	101.0	202.0	303.0	404.0	101.0	202.2	303.3	403.3	105.8	210.7	316.5	423.7

3. Comparison of experimental data with computational results

3.1. Rossiter formula for modal resonant frequencies

On the basis of his experimental results, Rossiter [24] suggested a semi-empirical formula for predicting the modal resonant frequencies for high subsonic compressible flows over shallow cavities. For a cavity with a large length-to-depth ratio $L/D \geq 1$, the Rossiter modal frequencies could be determined by using the empirical formula

$$f_n = \frac{U_\infty}{L} \frac{n - \gamma}{M + 1/\kappa}, \tag{6}$$

where n is the cavity mode, U_∞ is the free stream velocity, κ is the ratio of the vortex convection velocity to the free stream velocity, and γ is the time lag between the impingement of a vortex on the downstream corner and the emission of an acoustic wave. The empirical parameters, κ and γ, were adjusted to match the experimental data published by Rossiter [24]. He also reported that $\kappa = 0.57$ and $\gamma = 0.25$ for a cavity with a length-to-depth ratio of 4:1 at various free stream Mach numbers [24]. In a recent study, Delprat [25] confirmed that equation (6) provides reasonably accurate estimates of the resonant frequencies of buffeting noise. Table I shows the measured data of the Rossiter resonant frequencies for the first four modes. The predicted modal frequencies according to equation (6) with $\kappa = 0.57$ and $\gamma = 0.25$ are shown in Table I for comparison. The predicted modal frequencies were within 2.3% of the measured results.

Chatellier *et al.* [26] suggested that the retroaction due to the interaction of the shear layer and the impingement corner is instantaneous and that the associated parameter should be negligible and set at zero at low Mach numbers. Hence, parameter γ could be obtained from experimental data for a known flow condition. On the basis of the measured results for different mean flow velocities and modal resonant frequencies, our calculations suggested that κ had a mean value of 0.42 and a standard deviation of $3.8 \cdot 10^{-3}$.

3.2. Validity of computational model

Section 2.1 outlined a computational scheme to calculate the fluctuating pressures for a subsonic flow over a cavity. To establish its suitability and accuracy, we used the computational scheme to simulate the time histories of the fluctuating pressures inside the cavity. Figure 5 shows the time histories of the fluctuating pressures at the center of the cavity bottom for the mean flow speeds of 15 and 25 m/s. This location was selected to coincide with that used in the experimental measurements.

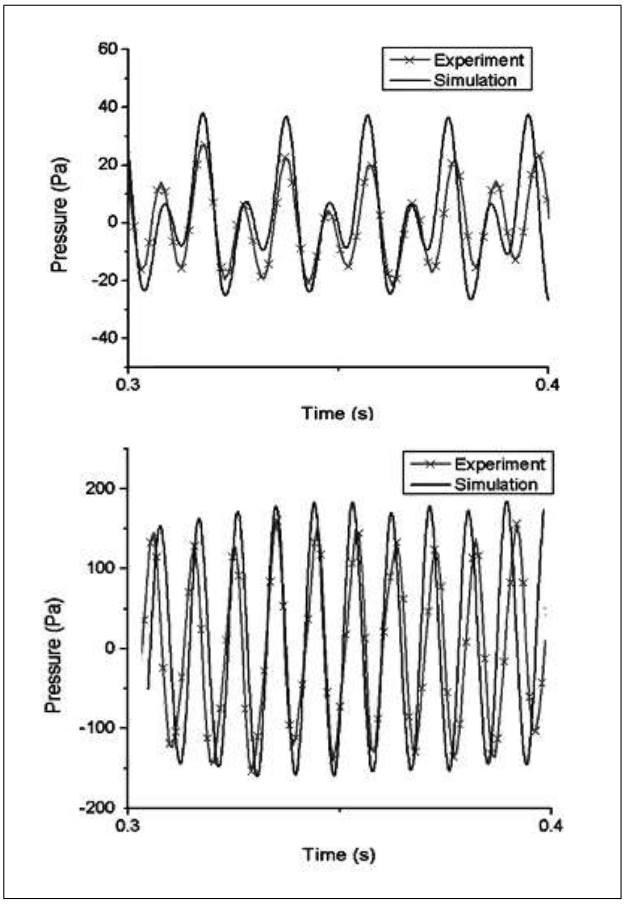

Figure 5. The pressure time histories at the center of cavity floor.

To obtain converged results, it is essential that the CFL criterion is met. In fact, the CFL number reflects the portion of a cell that a fluid traverses by advection in one time step. To improve the numerical accuracy, the Courant number should preferably be chosen to be less than 1.5 in order to reduce oscillations and the effect of numerical dispersion. In general, each cell in the computations has a different CFL number. A summary of statistical data used in our numerical simulations shows that over 95% of cells have CFL numbers that are less than 1.5. Typically, forty oscillations were calculated for obtaining the statistics of the time data.

The simulated acoustic pressures showed a strong periodicity that corresponded to a self-sustained pressure oscillation known as the wind buffeting noise. For the mean

flow speed of 25 m/s, the apparent period of the oscillation, T, could be determined as 9.4 ms, which was equivalent to a fundamental resonant frequency of 105.8 Hz. The measured data are also shown in Figure 5 for comparison with the computational results. In general, the numerical simulations overestimated the amplitude of the fluctuating pressure. This error may be caused by the difference in the boundary conditions applied at the cavity opening between the numerical simulations and experimental measurements. It is important to note in our numerical simulations that a uniform velocity profile with a turbulent intensity of 0.5% was assumed at the inlet of the flow field. Contrastingly, a turbulent boundary layer was expected in the experimental measurements where its characteristics were generally not available. Krishnamurthy [27] showed that the sound intensity induced by a laminar boundary layer was stronger than that due to a turbulent boundary layer. However, the acoustic pressure fluctuations are generally much larger than that caused by the vortex shedding itself. These acoustic pressure excitations are coupled with the resonant effect of the cavity. The impact of turbulent/laminar boundary layer on the wind buffeting noise is small. This can be confirmed by the fact that the computed results are in good agreement with the experimental data.

On the basis of the time histories of the fluctuating pressures, it was possible to convert the computed data to the frequency-domain results by a standard fast Fourier transform (FFT) routine. Figure 6 displays the computed and measured sound power spectra at the center of the cavity bottom for the mean flow speed of 25 m/s. Three resonant peaks – 105.8 Hz, 210.7 Hz, and 316.5 Hz – could be easily identified in the computed frequency spectrum. The first resonant peak was the fundamental frequency of the flow instability over the cavity. These predicted modal frequencies suggested that the fluctuating pressures had good harmonicity that agreed reasonably well with the Rossiter's formula, *cf* equation (6), and the measured data. Computations were also conducted for other flow speeds in order to obtain the corresponding modal resonant frequencies. Comparable sound power spectra could be obtained, but they are not shown here for brevity. Nevertheless, the simulated results for the modal resonant frequencies at three flow speeds (15 m/s, 20 m/s, and 25 m/s) are listed in Table I for information.

Note that the background noise levels were relatively high for the experimental data at low frequencies (see Figure 6). As a result, the agreement between the computed and the measured sound power spectra was relatively poor at low frequencies. This was because the computation model used in the present study did not include the simulation of the background noise.

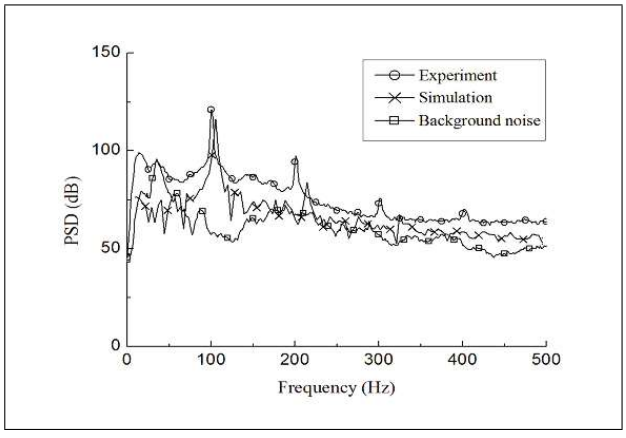

Figure 6. Comparison of predicted and measured sound power spectral density at the center of cavity bottom for Model A.

4. Passive control of wind buffeting noise

4.1. Prediction of pressure and vorticity contours over a cavity

The oscillation of the flow over a cavity is a resonance phenomenon. A design that can lead to a disruption of the resonance mechanism may be used for suppressing resonant tones, but in practice, it is a non-trivial effort to find an effective solution to control the buffeting noise [28] for a wide velocity range.

One of the more popular methods for suppressing the wind buffeting noise is to install a deflector at the leading edge of the cavity [29, 30, 7]. The presence of a deflector destroys vortex shedding at the leading edge of the cavity that reduces the buffeting noise. An alternative passive method is to change the size of the cavity opening [27, 31, 7]. In this method, the frequency of the resonant mode can be adjusted by varying the size of the opening so that the resonant effect can be avoided at a particular frequency. However, this alternative method will not be pursued in the present study.

Because of the high fidelity of the flow simulations and an accurate prediction of the resonant modal frequencies, it was possible to explore different designs for reducing the wind buffeting noise of a generic cavity. To aid the design process, we studied the characteristics of the flow instability over the cavity by considering the instantaneous vorticity ω where it is defined as the change in circulation $\delta\Gamma$ over a small region of fluid δA. In the limit of $\delta A \to 0$ (the region δA has been reduced to a single point), ω at this point is given by $\omega = \mathrm{d}\Gamma(\mathrm{d}A$. Figures 7 and 8 show the pressure contours and instantaneous vorticity for Model A. The numerical simulations for the mean flow speed of 25 m/s was selected for presentation. Numerical simulations for other low subsonic flow speeds showed rather similar results.

Plots 7a to 7h display the pressure contours at eight time intervals for one period with a time step of $T/8$ between the adjacent intervals. These snapshots of pressure contours explained the reason for a high level of buffeting noise at the cavity, which was recorded at an SPL of 115.4 dB and a resonant frequency of 105.8 Hz. A close examination of Figure 7 led to the following observations: At $t = 0$, a vortex with a low-pressure core was formed and began to shed at the leading edge of the open cavity. At $t = T/8$, $T/4$, and $3T/8$, the vortex was convected downstream, which led to a buildup of pressure in the cav-

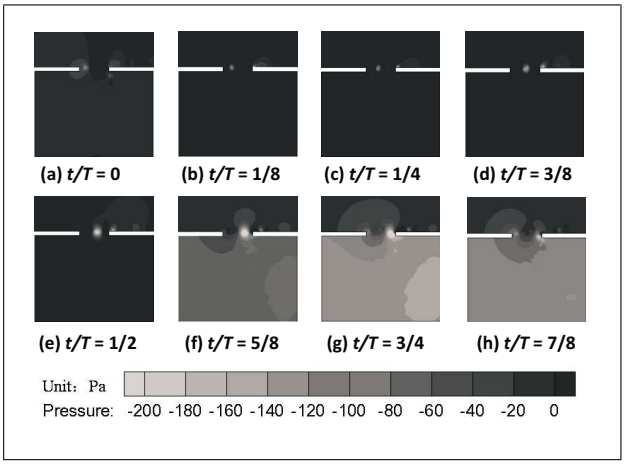

Figure 7. Instantaneous pressure contours at eight time instants.

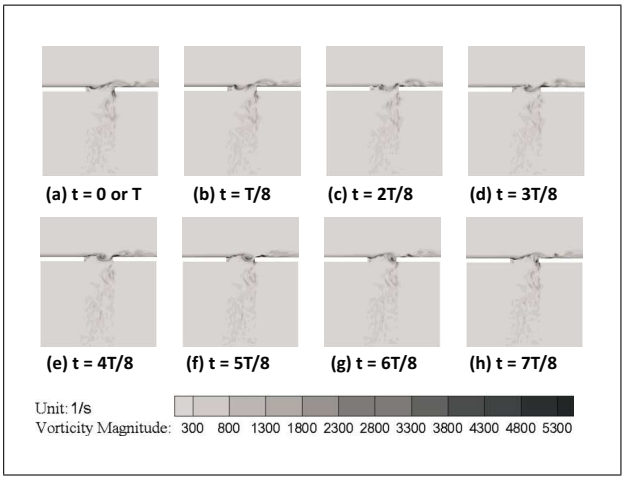

Figure 8. Instantaneous vorticity contours at eight time instants.

ity. The pressure of the vortex core was the lowest and the pressure in the cavity reached its maximum value at approximately $t = T/2$. The convected vortex hit the trailing edge of the cavity at approximately $t = 5T/8$. This interaction led to the breakdown of the vortex, causing a significant reduction in the interior pressure of the cavity. The process of disintegration of the vortex continued and the cavity pressure reduced to its lowest value at approximately $t = 3T/4$. The cavity pressure increased again at approximately $t = 7T/8$ because of the "spring back" of the pressure wave. The period ended at $t = T$, and the flow pattern returned to its initial state for the beginning of the next cycle.

Figure 8 shows the numerical simulations of the vorticity contours in eight snapshots within one oscillation period. The plots illustrate the periodic shedding of vortices at the leading edge of the cavity. These vortices were convected downstream by the boundary layer flow.

The instantaneous streamlines at $t = 3T/4$ were obtained to reveal the vortical structures developed inside the cavity (Figure 9). As shown in the plot, there was a large re-circulating flow at the center of the cavity coupled with smaller re-circulating regions on the right side

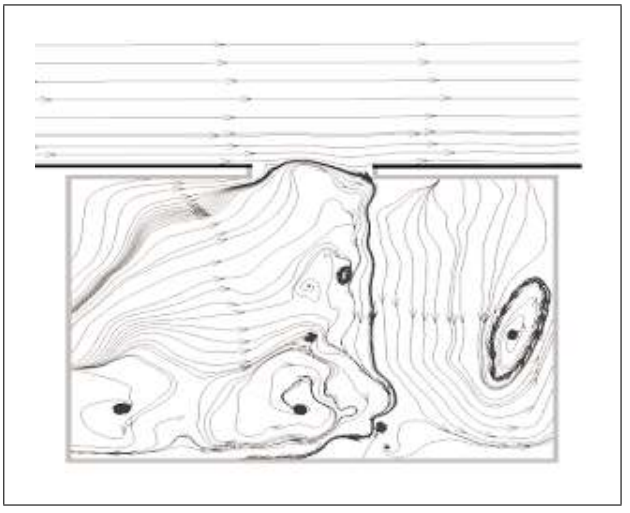

Figure 9. Instantaneous velocity streamlines at $t/T = 3/4$.

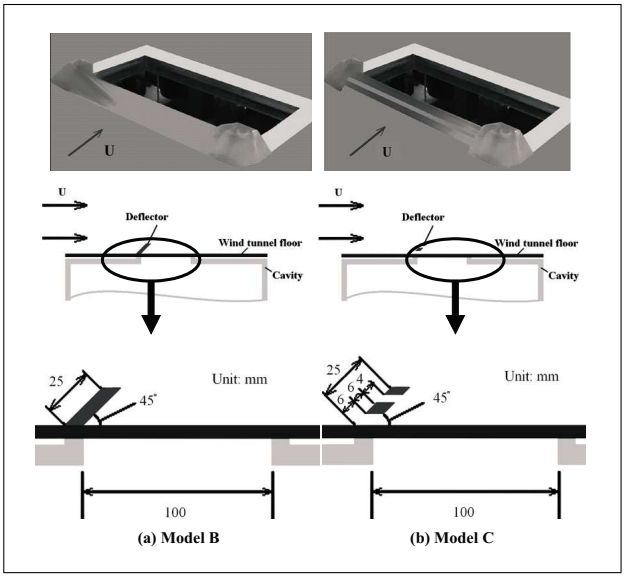

Figure 10. Two deflector models: Model B and Model C.

of the cavity. In the left corners, secondary re-circulating regions were formed, driven by the relatively large region in the center. The re-circulating flow caused the shedding of vortices and the instability in the shear layer behind the trailing edge of the cavity opening.

4.2. Reduction of wind buffeting noise by deflectors

With the aid of the numerical tool described earlier, two types of generic deflectors were designed to tackle the buffeting noise for the flow over the cavity. Figures 10a and 10b show the schematic representations of these two designs, which are referred to as Model B and Model C, respectively. Model B was a simple deflector that was designed to reduce the vortex shedding at the leading edge of the cavity. Model C was an improved design that was used for reducing the wind buffeting flow at relatively high mean flow speeds.

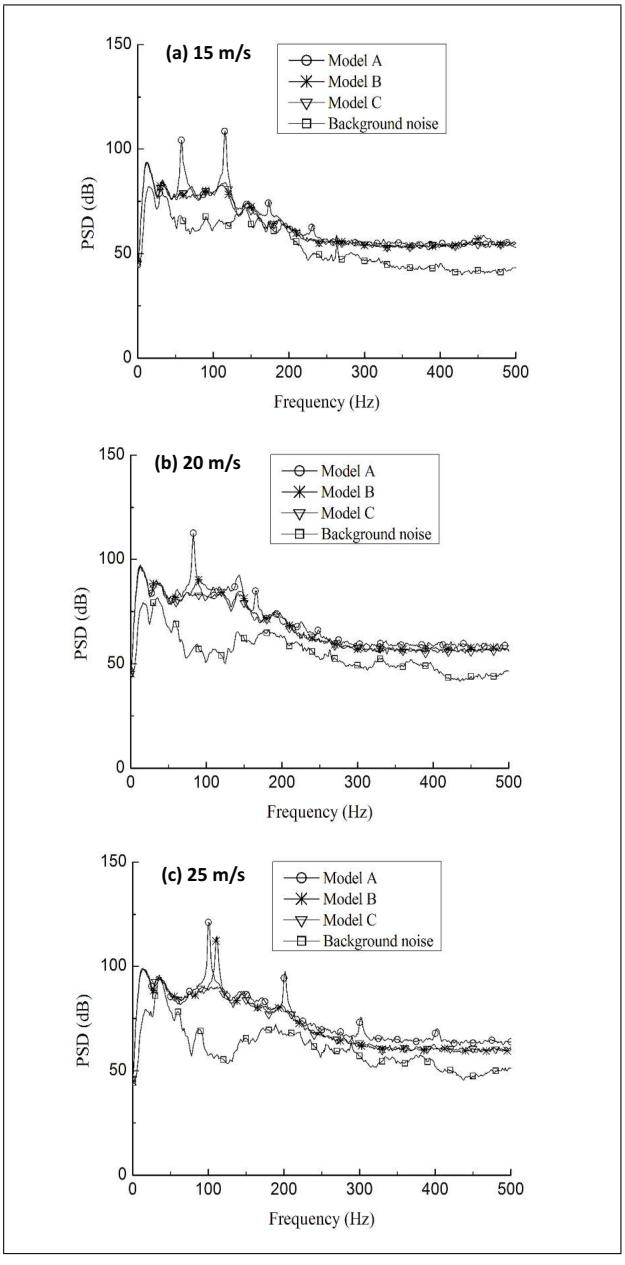

Figure 11. Power spectral density of measured pressure fluctuations at different velocities.

5. Effectiveness of deflectors for suppressing wind buffeting noise

Figure 11 shows three plots of the power spectral density (PSD) of measured pressures for three different free stream velocities at 15, 20, and 25 m/s. In each plot, the measured sound spectral densities for Models A, B, and C are shown. Further, the background noise levels are shown for reference. These background noise levels were measured separately when the wind tunnel was operated in the absence of the cavity at the respective flow speeds. The measured results for Model A (cavity without a deflector) confirmed the quasi-harmonicity of the fluctuating pressure [25]. However, different mean flow velocities induced different modal resonant frequencies.

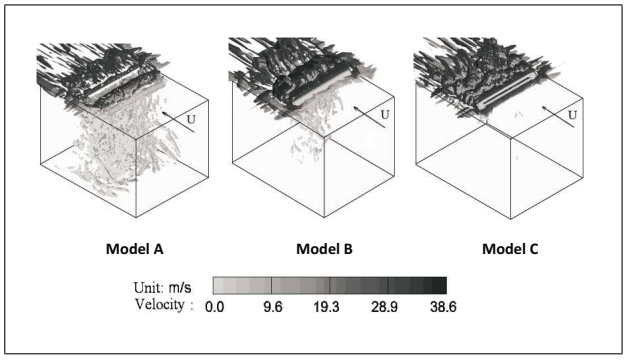

Figure 12. Instantaneous isosurfaces of Q for different models. Isosurfaces at $Q = 9750$ are shown and shaded with stream velocity, ranging between 0 and 30 m/s.

By adding a simple deflector (Model B), we demonstrated that the buffeting noise can be effectively suppressed for the mean flow speeds of 15 and 20 m/s (see Figures 6a and b). However, when the flow speed was increased to 25 m/s, Model B offered noise reduction at the original fundamental frequency of 101 Hz at the expense of introducing another modal resonant frequency of 119.3 Hz. However, the design of the deflector in Model B did not provide an effective means of reducing the wind buffeting noise.

An improved design of the deflector, Model C, was then developed on the basis of the idea of "venting." Model C was explored by introducing a vent in the deflector for controlling the buffeting noise. Figure 10b shows the design of the vented deflector. The experimental results for Model C at the three mean flow speeds are also shown in Figure 11. We could see that this improved design was effective in reducing the wind buffeting noise even at a mean flow speed of 25 m/s, at which Model B was not effective.

To understand the noise reduction mechanism of the vented deflector, it is instructive to show the detailed numerical analyses that were used for finalizing the design. It should be mentioned that the maximum flow speed of the wind tunnel was 25 m/s.

To understand the effect of deflectors on the shedding of vortices, the second invariant of the velocity gradient tensor, Q, was introduced; Q is defined as

$$Q = \frac{1}{2}\left(\Omega_{ij}\Omega_{ji} - S_{ij}S_{ji}\right), \tag{7}$$

where the vorticity tensor Ω_{ij} and the rate of strain tensor S_{ij} are, respectively, given by

$$\Omega_{ij} = \frac{1}{2}\left(\frac{\partial u_j}{\partial x_i} - \frac{\partial u_i}{\partial x_j}\right) \tag{8a}$$

and

$$S_{ij} = \frac{1}{2}\left(\frac{\partial u_j}{\partial x_i} + \frac{\partial u_i}{\partial x_j}\right). \tag{8b}$$

The so-called Q criterion [32] was chosen for the detection of the vortices in the numerical simulations.

Figure 12 shows the instantaneous isosurfaces of Q for different models ($t = T/4$). The deflector was designed to

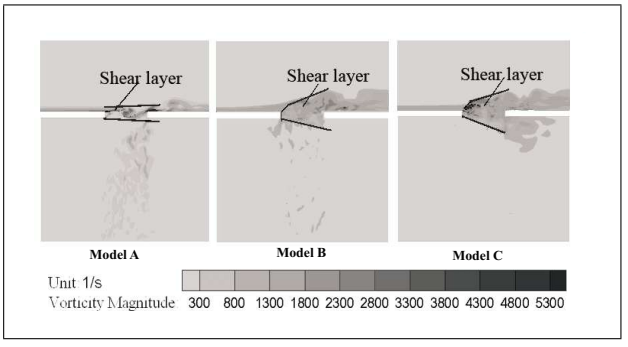

Figure 13. Instantaneous vorticity distribution around the cavity.

reduce the shedding of vortex by the leading edge of the cavity mouth, and the velocity gradient inside the cavity itself was considerably small. As a result, there were few small vortex structures generated inside the cavity when a new deflector was installed.

Figure 13 shows the distribution of instantaneous vorticity and the structures of the shear layer near the cavity openings ($t = T/4$). The shear layer in Model C had the widest distribution of flow instabilities near the opening but a narrower distribution in the cavity. Contrastingly, the shear layer in Model A induced few flow instabilities at the opening, but it created more vorticity structures inside the cavity. Finally, the vorticity structure of Model B lay somewhere between those of Models A and C. From the viewpoint of energy conservation, the deflector provided effective dissipation of energy at the opening, which led to reduced energy dissipation in the cavity. Hence, the presence of a deflector at the opening of the cavity could not trigger strong pressure fluctuations inside the cavity. A vented deflector (Model C) can lead to even more energy dissipation at the cavity opening, as illustrated in Figure 13. This phenomenon echoed the conclusion of Krishnamurthy [27] in that the sound intensity induced by a turbulent boundary layer is weaker than that due to a laminar boundary layer.

Figures 14 and 15 show snapshots of the instantaneous pressure contours for Models B and C, respectively. These simulated results suggested that there existed strong vortex shedding and pressure fluctuating in Model B, but there was a relatively weaker pressure fluctuating in Model C.

As demonstrated in Figures 12, 14 and 15, the vent slots on model C modified the flow structure of the shear layer significantly such that the unsteady vortex structures shed from the deflector were directed towards the outside of the cavity. In the contrast, there were still certain amounts of vortices shed into the cavity as shown in Figure 12 for model B. This flow control mechanism contributes to the reduction of buffeting noise in model C. This can be confirmed by experimental and numerical results as follows. Figure 16 shows the predicted and measured sound power spectra at the monitoring point for Models B and C for a mean flow speed of 25 m/s. The simulation results agreed well with the experimental results for both the deflectors. There was no resonant peak in the power spectrum of Model C, which implied that the wind buffeting noise in

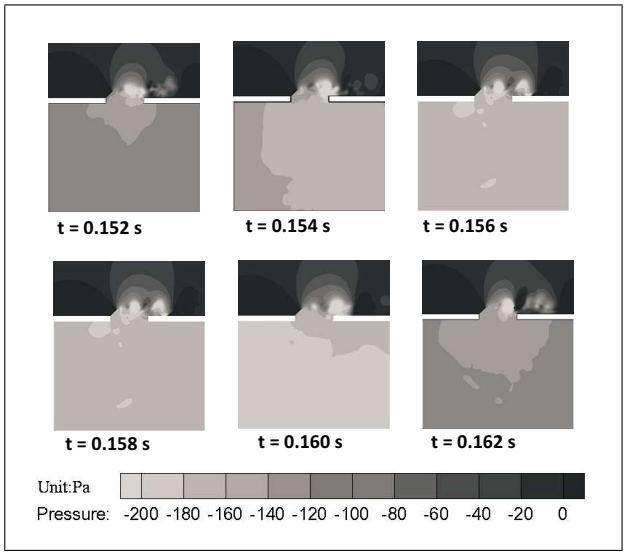

Figure 14. Instantaneous pressure fluctuations for Model B.

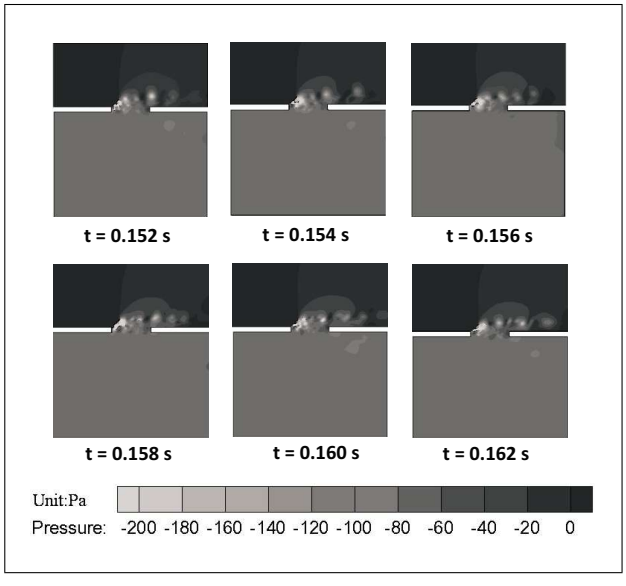

Figure 15. Instantaneous pressure fluctuations for Model C.

the cavity was effectively suppressed by the vented deflector.

6. Conclusion

In this study, we demonstrated that a set of incompressible Navier–Stokes equations could be used for simulating the flow over a cavity. An assumption of a weak compressibility effect was also required as it allowed the introduction of a source term in the continuity equation. The application of this computational scheme led to a high-fidelity simulation of the flow over a cavity with and without a deflector. It allowed a reasonable prediction of modal resonant frequencies that were in good agreement with the Rossiter formula.

More importantly, the present study exemplified the usefulness of computational fluid dynamics (CFD) in aircraft and automobile design. In particular, CFD was ap-

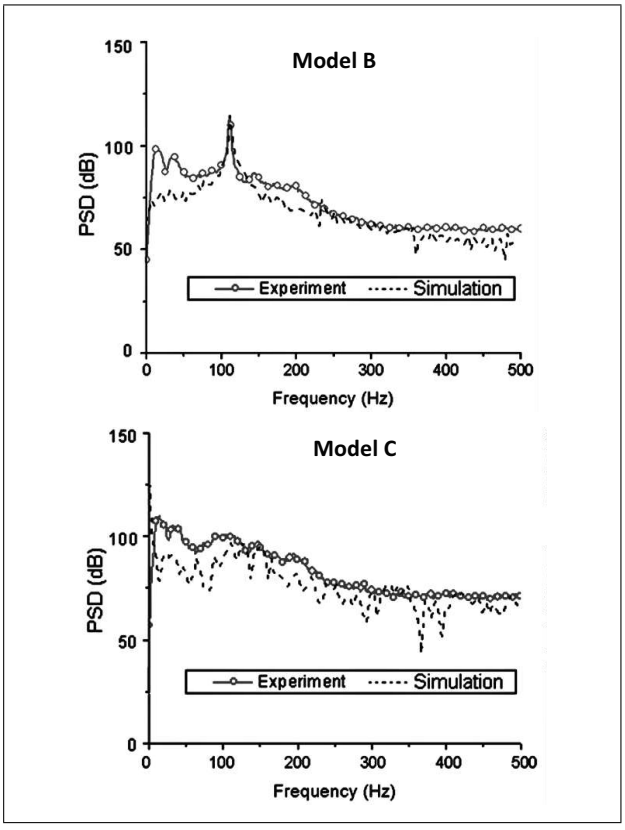

Figure 16. Power spectra of pressure fluctuation at the center of the cavity floor for Models B and C at a mean flow speed of 25 m/s.

plied to design a generic vented deflector for reducing the wind buffeting noise in an open cavity. Numerical simulations were used for comparing the flow fields and flow instabilities induced by the shedding of periodic vortices at the leading edge of the cavity. This better understanding of flow fields led to a better design of a vented deflector for reducing the wind buffeting noise at high flow speeds. In the present study, the vented deflector showed superiority in the reduction of the wind buffeting noise by modifying the flow structure of the shear layer. The sharp edge of the slot used in the present study may increase the broad-band noise levels, particularly, at the high-frequency range. Future study should be directed to a comprehensive evaluation and a better understanding of the vented deflector for reduction of the wind buffeting noise in cavities.

Acknowledgement

The research was conducted while YPW was a visiting scholar at the Ray W. Herrick Laboratories, Purdue University. YPW gratefully acknowledges the financial support from China Scholarship Council of the National Natural Science Foundation

References

[1] S. Hein, T. Hohage, W. Koch: Acoustic resonances in a high-lift configuration. Journal of Fluid Mechanics **582** (2007) 179–202.

[2] Y. P. Guo, K. J. Yamamoto, R. W. Stoker: Experimental study on aircraft landing gear noise. Journal of Aircraft **43** (2006) 306–317.

[3] C. Y. Loh: Computation of low speed cavity noise. AIAA paper 2004-0680, 2004.

[4] B. Crouse, S. Senthooran, G. Balasubramanian: Computational aeroacoustics investigation of automobiles sunroof buffeting. SAE paper 2007-01-2403, 2007.

[5] H. S. Kook, S. R. Shin, G. D. Ih: Measurement of the sunroof buffeting noise with an automatic deflector-traversing device. International Journal of Precision Engineering and Manufacturing **11** (2010) 5–11.

[6] P. E. Slaboch, S. C. Morris, R. Ma: Window buffeting measurements of full-scale vehicle and simplified small scale models. SAE paper 2009-01-0181, 2009.

[7] C. F. An, K. Singh: Optimization study for sunroof buffeting reduction. SAE paper 2006-01-0138, 2006.

[8] M. Inagaki, K. Abe, T. Kondoh: Numerical prediction of fluid-resonant oscillation at low mach number. AIAA Journal **40** (2002) 1823–1829.

[9] D. Rockwell, E. Naudascher: Review: Self-sustaining oscillations of flow past cavities. Journal of Fluids Engineering **100** (1978) 152–165.

[10] Exa Corporation. http://www.exa.com/pages/pacoustics/poweracoustics_main.html, 2010.

[11] H. China, T. Kataoka, M. Yoshida: Simulation of interface oscillation phenomenon over a cavity in air flow, advances in numerical simulation of turbulent flows. Proceedings of the First Joint ASME-JSME Fluid Engineering Conference, FED-119, American Society of Mechanical Engineers, 1991, 71–76.

[12] C. F. An, S. M. Alaie, D. S. Sandeep: Side window buffeting characteristics of an SUV. SAE paper 2004-01-0230, 2004.

[13] E. Turkel: Review of preconditioning methods for fluid dynamics. Applied Numerical Mathematics **12** (1993) 257–284.

[14] D. V. Brown, L. Mongeau: The design, construction, and validation of a small, low-speed, quiet wind tunnel with application to noise from the flow over a cavity. Ray W. Herrick Laboratories Internal Report No. 204, Purdue University, West Lafayette, Indiana, 1995.

[15] H. Kook, L. Mongeau, D. V. Brown: Analysis of the interior pressure oscillations induced by flow over vehicle openings. Noise Control Engineering Journal **45** (223-234) 1997.

[16] S. Pope: Turbulent flows. Cambridge University Press, Cambridge, UK, 2000.

[17] J. Smagorinsky: General circulation experiments with the primitive equations. I. The basic experiment. Monthly Weather Review **91** (1963) 99–164.

[18] R. I. Issa, A. D. Gosman, A. P. Watkins: The computation of compressible and incompressible recirculating flows by a non-iterative implicit scheme. J. Comp. Phys. **62** (1986) 66–82.

[19] I. Orlanski: A simple boundary condition for unbounded flows. Journal of Computational Physics **21** (1976) 251–269.

[20] M. Breuer: Large-eddy simulation of the sub-critical flow past a circular cylinder: Numerical and modeling aspects. International Journal for Numerical Methods in Fluids **28** (1998) 1281–1302.

[21] M. Breuer: A challenging test case for large-eddy simulation: High Reynolds number circular cylinder flow. International Journal of Heat and Fluid Flow **21** (2000) 648–654.

[22] M. Wang, P. Catalano, G. Iaccarino: Prediction of high reynolds number flow over a circular cylinder using LES with wall modeling. Center for Turbulence Research Annual Research Briefs, 2001.

[23] H. Werner, H. Wengle: Large eddy simulation of turbulent flow over and around a cube in a plate channel. Proceedings of the 8th Symposium on Turbulent Shear Flows, 1991, 1941–1946.

[24] J. E. Rossiter: Wind tunnel experiments on the flow over rectangular cavities at subsonic and transonic speeds. Aeronautical Research Council Reports and Memo No. 3438, 1964.

[25] N. Delprat: Rossiter's formula: A simple spectral model for a complex amplitude modulation process? Physics of Fluids **18** (2006) 071703–1–071703–4.

[26] L. Chatellier: Modélisation et contrôle actif des instabilités aéroacoustiques en cavité sous écoulement affleurant. These, Université de Poitiers (in French), 2002.

[27] K. Krishnamurty: Acoustic radiation from two-dimensional rectangular cutouts in aerodynamic surfaces. NACA, Tech. Note 3487, pp. 1–33, 1955.

[28] C. W. Rowley, D. R. Williams: Dynamics and control of high-reynolds-number flow over open cavities. Annual Review of Fluid Mechanics **38** (2006) 251–276.

[29] K. J. Karbon, R. Singh: Simulation and design of automobile sunroof buffeting noise control. 8th AIAA/CEAS Aeroacoustic Conference and Exhibit, Breckenridge, Colorado, 2002, 2002–2550.

[30] D. K. Ota, S. R. Chakravarthy, T. Becker: Computational study of resonance suppression of open sunroofs. Journal of Fluids Engineering **116** (1994) 877–882.

[31] V. Sarohia: Experimental investigation of oscillations in flows over shallow cavities. AIAA Journal **15** (1977) 984–991.

[32] J. C. R. Hunt, A. A. Wray, P. Moin: Eddies, stream, and convergence zones in turbulent flows. Proceedings of the Summer Program, Center of Turbulence Research, Stanford, CA, 1988, 193–207.

[33] G. Ashcroft, X. Zhang: Vortical structures over rectangular cavities at low speed. Physics of Fluids **17** (2005) 015104–1–015104–8.

[34] M. Daoud, A. M. Naguib, I. Bassioni: Microphone-array measurements of the floor pressure in a low-speed cavity flow. AIAA Journal **44** (2006) 2018–2023.

[35] N. Frorestier, L. Jacquin, P. Geffroy: The mixing layer over a deep cavity at high subsonic speed. Journal of Fluid Mechanics **475** (2003) 101–145.

[36] M. Gharib: The effect of flow oscillations on cavity drag, and a technique for their control. Ph.D. Thesis, California Institute of Technology, 1983.

[37] M. Inagaki, O. Murata, N. Horinouchi: Numerical prediction of wind-throb noise in vehicle cabin. Proceedings of 6th World Congress on Computational Mechanics in conjunction with the Second Asian-Pacific on Computational Mechanics, 2004, 105–112.

[38] M. A. Kegerise, E. Spina, S. Garg: Mode-switching and nonlinear effects in compressible flow over a cavity. Physics of Fluids **16** (2004) 678–687.

[39] L. Larcheveque, P. Sagaut, I. Mary: Large-eddy simulation of a compressible flow past a deep cavity. Physics of Fluids **15** (2003) 193–210.

[40] D. Rockwell, C. Knisely: Vortex-edge interaction: Mechanisms for generating low frequency component. Physics of Fluids **23** (1980) 239–240.